Mine Water and the Environment (2022) 41:518–532
https://doi.org/10.1007/s10230-022-00854-x

TECHNICAL ARTICLE

Chemometrics in Ascertaining Hydrogeochemical Characteristics of Coal Mine Discharge vis-à-vis Behaviour of Surface and Groundwater Resources of the Mahan River Catchment Area, Central India

Nirmal Kumar[1] · Mahendra Kumar Tiwari[2] · Rambabu Singh[3] · Abhay Kumar Singh[4]

Received: 3 July 2021 / Accepted: 14 February 2022 / Published online: 28 February 2022

Abstract
We investigated the hydrogeochemical regime of an AMD-affected coal mining province. 98 water samples were collected over two seasons and analysed for 14 parameters. We attempted to discriminate the sources of variation of water quality using select multivariate techniques: display methods (principal component analysis) and unsupervised pattern recognition (cluster analysis). Most of the groundwater and river water were characterised by shallow freshwater facies (Ca–Mg–HCO_3 type), whereas the samples representative of mine water were of the Ca–Mg–SO_4 type. The mines of the area annually discharge 2901 t of solute loads, ranging from 91 to 1030 t/year. Various molar ratios suggest that dissolution of the silicates associated with the mixing process is the predominant solute acquisition processes that govern the water chemistry of the region besides AMD. The chemometric results indicated that only a few groundwater and river water samples had low pH and elevated total dissolved solids, and these were near the three mines that were affected by AMD. These results substantiate the effectiveness of the mine water treatment measures implemented at the mine sites.

Keywords Mine water · Acid mine drainage · Elemental flux · Hydrogeochemistry · PCA · HCA

Introduction

In India, 89% of the extracted groundwater is used by the irrigation sector, after which 9% is domestically used and only 2% is used by industry (Singh et al. 2021a; Suhag 2016). The demands on this water are growing, and many scientists prognosticate that a shortage of fresh water is imminent for many reasons, including rising water demands of the rapidly growing population coupled with urbanization, industrialization, and intensive agricultural activities (Singh et al. 2021b). All of these have the potential to impact groundwater quality as well as its quantity (Kumar et al. 2018, 2019; Wagh et al. 2019). However, coal mining is an indispensable part of India's development in general, and its power sector development in particular (Singh et al. 2017a, b). In the process of coal mining, large volumes of water gets collected in mine sumps and subsequently pumped to the surface (Mahato et al. 2017). This mine water can be an immensely valuable asset, if treated and used appropriately for domestic, agriculture, industrial, and recreational use (Singh et al. 2018).

Sometimes, the discharged mine water is acidic in nature, due to the oxidation of sulphur-bearing minerals like pyrite, marcasite, and pyrrhotite (Ray and Dey 2020). Since coal mining by both opencast and underground methods affects the environment of the area, the study of groundwater chemistry in such areas is crucial for assessing the comparative importance of anthropogenic and natural processes in defining the quality of groundwater (Acharya and Kharel 2020).

✉ Rambabu Singh
rambabu.singh@coalindia.in

[1] Mining Department, South Eastern Coalfield Ltd, Bilaspur, Chhattisgarh 495006, India

[2] Department of Environmental Science, AKS University, Satna, Madhya Pradesh 485001, India

[3] Exploration Department, Central Mine Planning and Design Institute Ltd, Bilaspur, Chhattisgarh 495006, India

[4] Central Institute of Mining and Fuel Research (Council of Scientific and Industrial Research), Dhanbad 826015, India

The present investigation was undertaken to evaluate the impact of coal mines on the water quality of the Mahan River catchment area, in the Surajpur districts of Chhattisgarh state, central India. There are six operating underground (UG) and opencast (OC) mines in this study area. These mines discharge treated mine drainage water into the surface drainage system. The Mahan River is a prominent tributary of the Son River and it is therefore appropriate to assess how these mines are affecting the aquatic environment (i.e. both groundwater and surface water) of the study area. The objectives of this study encompassed: (1) determining the hydrochemical evolution of groundwater in and around the coal mine provinces, (2) assessing seasonal fluctuations of the major ion chemistry and its spatial distribution in the area using statistical approaches, (3) understanding the impact of AMD on the surrounding water bodies, and (4) identifying the possible sources of various ions present in the groundwater using chemometric methods.

Geological and Hydrogeological Framework

Study Area

The study area is located in the central part of the Bishrampur coalfield, bounded by latitudes 23° 00′ N and 23° 30′ N and longitudes 83° 00′ E and 83° 45′ E (part of the Geological Survey of India (GSI) toposheet no. 64 I/15, 64 I/15, 64 M/3, 64 M/4, 64 M/7, and 64 M/8) is shown in Fig. 1. The area is well connected to the other collieries of the Bishrampur coalfield viz., Mahan-II OC, Bhatgaon UG, Mahamaya UG, Dugga UG, Mahan OC, Kalyani UG, Shivani UG, and Nawapara UG by all-weather roads. The Mahan River and its tributaries (Fig. 1) primarily control the drainage of this part of the coalfield. The topography of the area shows gently undulating trends with altitudes ranging from 446 to 672 m. The area, in general, has a tropical monsoon type of climate, which is characterized by heavy rainfall during the monsoon, with hot summers and cold winters. The annual mean daily temperatures range between 17.8 and 30.1 °C.

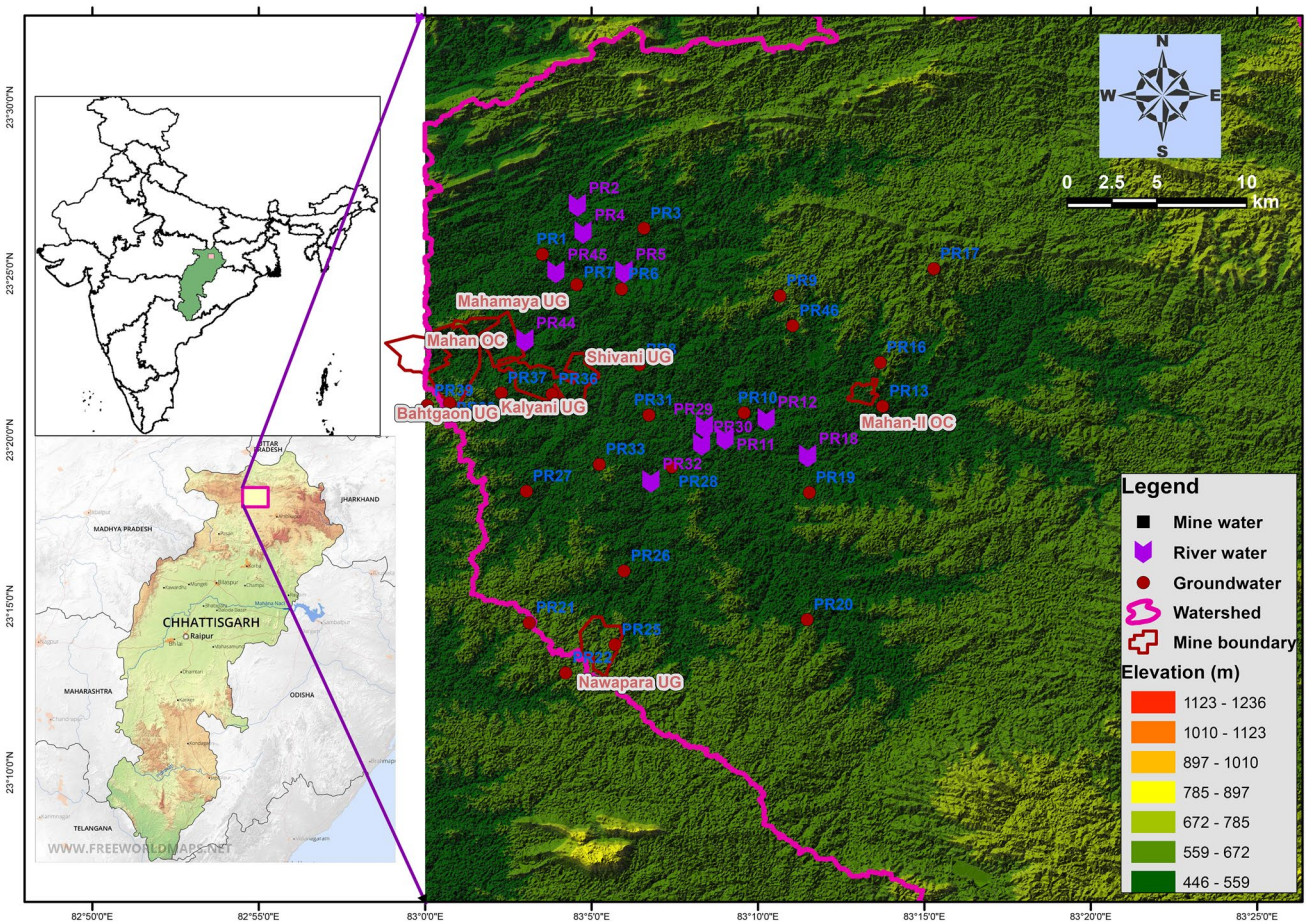

Fig. 1 Location map of the study area showing the sampling sites and elevation pattern

Mean monthly temperature is highest in the month of May (42.7 °C) while the mean monthly temperature is lowest in the month of January (4.4 °C). The wettest months are June to September when more than 87% of the annual rainfall occurs. The average annual rainfall from 1991 to 2017 was about 1270 mm.

Tectonically, the Son-Mahanadi basin is divided into three sub-basins with the Son sub-basin in the north, Mahanadi sub-basin in the south, and Hasdeo-Arand sub-basin in the central part occupying the drainage areas of the Son, Hasdeo, and Mahanadi Rivers (Agarwal et al. 1993). In the Son-Mahanadi basin, Gondwana sediments of the Talchir, Barakar and Kamthi Formations, rest either unconformably or with faulted contact over the Pre-Cambrian crystalline basement in the northern and eastern parts (Table 1). The coal basin has a faulted contact with the Proterozoic Cuddapah/Chhattisgarh rocks in the south and southwestern part. Inliers of crystalline rock are numerous in this area. The Bishrampur coalfield is rectangular in shape and extends nearly 37 km from east to west and 34 km from north to south, and occupies the north-eastern corner of the Hasdeo-Arand sub-basin. The adjacent Lakhanpur coalfield and Bisrampur coalfield form twin basins in the eastern part of the Son Valley and are inter-connected by a narrow strip of Talchir Formation.

The Bishrampur coalfield belongs to the Lower Gondwanas formations, which are represented by Talchirs, Karharbaris, Barakars, and Kamthis. The Barakar sediments, which are the only coal-bearing formation in this area, occurs in a rectangular outcrop. The Talchir rocks are exposed along the eastern and western peripheries, whereas towards the north and south, the Lower Gondwana sediments are juxtaposed with Archaean gneisses, slates, and quartzites. Younger sediments, probably representing the Kamthi Formation, occur at the higher contours in the Pilka Hill to the south. The stratigraphic succession of strata in the Bishrampur coalfield, as established by the GSI, is provided in Table 1.

In terms of the hydrogeology of the study area, major portions of the study area are covered by Barakar formation, comprises of soil cover and sandstone of different grain sizes with shale beds and coal seams. The Barakars, comprising medium to very coarse-grained sandstone with number of intervening gritty pebbly (conglomerate) horizons are saturated and behave as aquifers, while the shale beds and coal seams behave as aquicludes, producing a multi-layered aquifer system. The formation immediately above the working seam is comprised mainly of alluvium and sandstone (average thickness 16 m) and behaves as an unconfined aquifer while lower formations, consisting of compact sandstone with secondary porosity behave as semi-confined/confined aquifers. The aquifer parameters, as evaluated in the study area, are hydraulic conductivity (K) = 0.61 m/day, transmissivity (T) = 14 m^2/day, and storage coefficient (S) = 3.7×10^{-2}. However, at certain locations, the permeability is very high due to the presence of localized gritty/pebbly conglomeratic beds.

Materials and Methods

Sampling and Chemical Analysis

High-resolution sampling was intensely carried out to include all possible sources including mine water, groundwater, and river water from locations in and around the Mahan River catchment area of the Bishrampur coalfield (Fig. 1). A total of 96 water samples were collected during two field campaigns in pre- (May 2018) and post-monsoon seasons (November 2017). Additionally, two more buffer samples from a different, pollution-free watershed with

Table 1 The generalized stratigraphic sequence of the Bishrampur Coalfield

Age	Formation	Thickness (m)	Lithology as per GSI
Recent/sub recent	Alluvium		Soil and sub-soil
Unconformity			
Early Eocene/Cretaceous (?)	Dolerite Intrusive		Dolerite
Unconformity			
Lower Triassic to Upper Permian	Kamthi (?)	100	Ferruginous conglomeratic sandstone (100 m)
Lower Permian	Barakar	45–422	Feldspathic sandstones with pebbly bands, carbonaceous and grey shale clay beds, and coal seams (45–304 m)
	Karharbari	5–105	Coarse-grained sandstone with reworked Talchir clasts and conglomerate lenses, shale, and thin coal seam (5–105 m)
Upper Carboniferous	Talchir	1.5–269	Fine grained sandstones, olive green shale, silt stones, boulder beds, and diamictites
Unconformity			
Archaean	Metamorphic Basement		Granite gneisses, schists, quartzites, slates, phyllites and amphibolites

greater altitude (i.e. Mainpat) were collected during the pre-monsoon season to assess the intensity and impact of mining on the water of the study area. The water samples were collected in 500 ml narrow necked high density polyethylene bottles and filtered with 0.45 µm membrane filter paper using a vacuum pump. The filtered samples were stored at 4 °C without acidification and thereafter shifted to the laboratory for analysis.

The pH, electrical conductivity (EC), and total dissolved solids (TDS) of all of the water samples were recorded in situ using a portable multi-parameter tool kit (SPECTRO, SLE-2603). The major anions: chlorine (Cl^-), nitrate (NO_3^-), sulphate (SO_4^{2-}), fluorine (F^-) and major cations: calcium (Ca^{2+}), magnesium (Mg^{2+}), sodium (Na^+), potassium (K^+) were respectively analysed at CSIR—Central Institute of Mining and Fuel Research, Dhanbad, India using ion chromatography (Dionex Dx-120) and atomic absorption spectrometry (Varian, 280 FS) in the flame mode. The bicarbonate (HCO_3^-) concentration was determined by acid titration, while total hardness (TH) and total alkalinity (TA) were computed using analytical data and standard empirical formulas. The whole analysis was carried out by following the standard procedures of the American Public Health Association (APHA 2012). The quality assurance and quality control (QA/QC) of water sample measurements were assured by running a known standard after every 15 samples and the per cent relative standard deviation (RSD) as a representative of precision of the analysis was less than 5% for all samples. The calculated charge balance error (CBE) for analysed water samples was within the acceptable limit of ± 5%.

Chemometric Methods

The potential source of pollutants and their distribution in the multidimensional space and time was appraised using principal component analysis (PCA) and both R and Q-mode hierarchical cluster analysis (HCA). Prior to performing any multivariate statistical analysis, it is legitimate and proper to run a statistical test to point out outliers, normality, linearity, and homoscedasticity of data (Kumar et al. 2018). For this purpose, data is standardized through log transformation and brought onto the SPSS v17.0 statistical platform. Subsequently, the data is standardized to their corresponding z-scores to eliminate the influence of different units between variables (Tziritis et al. 2016).

Initially, PCA was chosen as it reduces the dimensionality of a data set consisting of a large number of interrelated variables without losing much of the essence of the important variables data. The limited components provided by the PCA help determine the variation trends of the data and plausible sources of the contaminants. First, though, the Kaiser–Meyer–Olkin (KMO) of sampling adequacy (cut-off above 0.50) and Barlett's tests of sphericity (significant level of $p < 0.05$) were checked to confirm that the selected variables had patterned relationships and were appropriate for PCA. The principal components were extracted after referring to the scree plot, which was constructed based on a measure of the significance of the component (i.e. eigenvalue > 1). The component loadings were optimized using the varimax (orthogonal) rotation method to attain simplified rotated components with the grouping of the most highly correlated variables governing the groundwater chemistry. The component loadings and their significance were classified as strong (> 0.75), moderate (0.75–0.50), and weak (0.50–0.30), regardless of sign.

Furthermore, agglomeration schedule statistics and linkage distance-based HCA was done to classify the variables or samples parameters into groups or facies based on their similarity with each other, relationship, and degree of contamination. Clusters of cases or samples highlight spatial relationships among the sample points rather than the parameters or variables; this procedure is often referred to as Q-mode HCA. The converse is true for R-mode HCA, which is generally done by classifying the parameters into groups based on their similarity with each other. By convention, a combination of the squared Euclidean distance as a similarity/dissimilarity measure among parameters, computed from Eq. (1) and Ward's agglomeration scheme, was chosen to link clusters/groups (Singh et al. 2017a).

$$d_{xy} = \sum_{j=1}^{p} (x_j - y_j) \quad (1)$$

where d_{xy} is the squared Euclidean distance between points x and y in p-dimensional space, and j defines each parameter. Subsequently, the sub-clusters were grouped to the main cluster in order to yield optimal groups for better interpretation. Finally, the results were transformed onto a dendrogram plot which provides a visual summary of clustering process and illustrate the relationships revealed by the HCA.

Results and Discussion

Ionic Dominance of the Various Water Sources and Implications on Health

A statistical summary of the water samples collected from groundwater (GW), river water (RW), and mine water (MW) during pre- (May 2018) and post-monsoon (November 2017) seasons is provided as a box plot. Figure 2 shows that in terms of ionic dominance, the pre-monsoon samples were all greater than those of the post-monsoon season and follow the order MW > RW > GW. The significant variation in the concentrations of measured hydrochemical parameters:

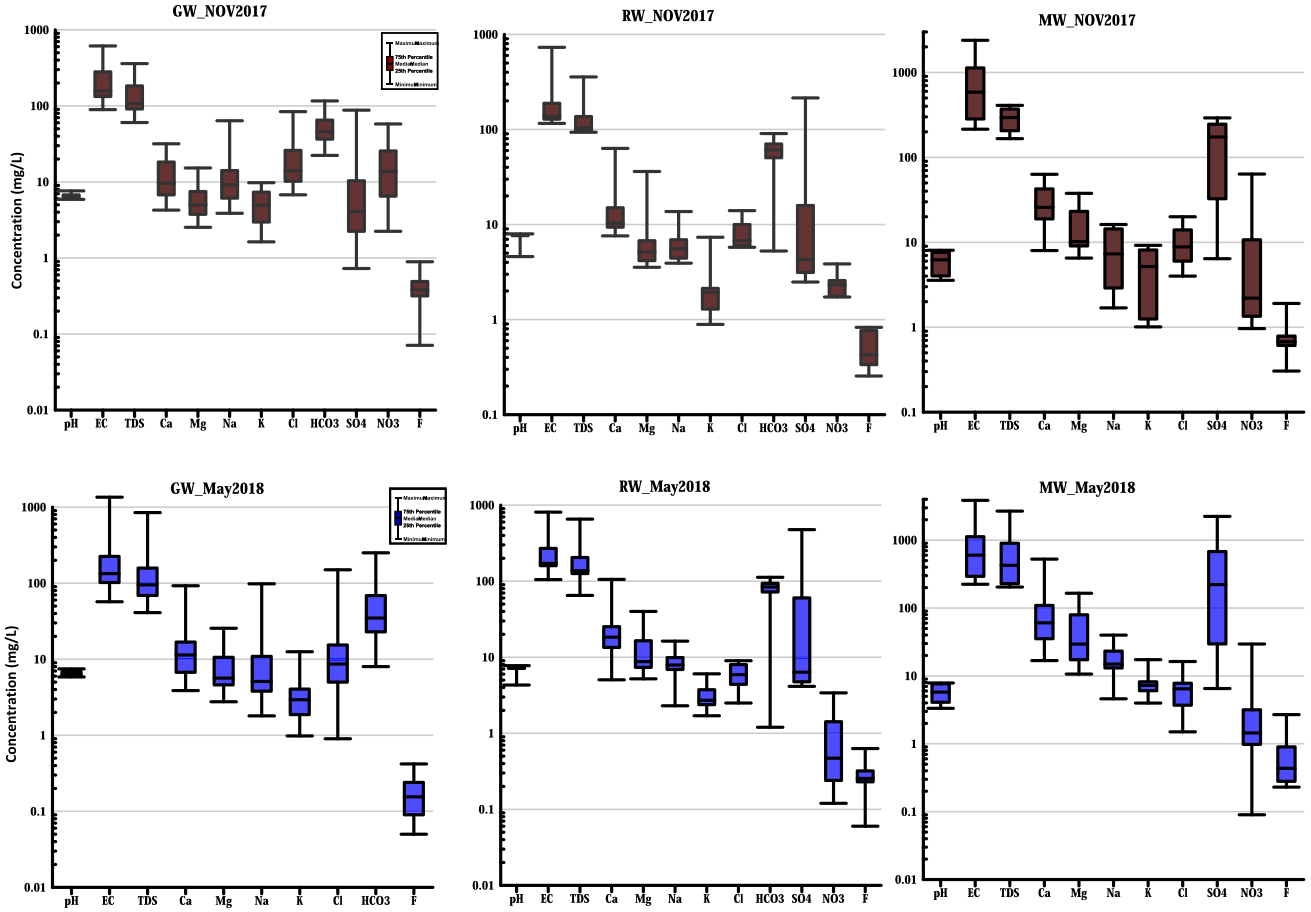

Fig. 2 Box plot illustrating the seasonal variation of the major ion chemistry for different water sources [All parameters are in mg/L except pH and EC (µs/cm)]

i.e. the ascendency of major ion concentrations in the pre-monsoon over the post-monsoon season is attributed to seasonal variation. This can be explained by various controlling factors, such as evaporation, intensive agricultural activity (sugar cane production), and mining activity, which have escalated concentration of major ions in these water sources during the pre-monsoon, whereas the comparative lower concentrations reported during the post-monsoon season are attributed to ample rainfall in the study area that helps to replenish the dynamic groundwater resource and dilutes contamination.

Descriptive statistics like minimum, maximum, and % of samples above the drinking water permissible limit (BIS 2012) are given in Table 2. In general, the physicochemical parameters of most of the water samples except for pH, were within the permissible limits during both post- and pre-monsoon seasons. Pre-monsoon, 48% of the water samples fall below the acceptable pH (6.5), compared to 44% in the case of the post-monsoon season. Water from these locations has a taste problem and corrosion effect when transported through mild steel and galvanized iron pipes. Similarly, 4% of the water samples in the pre-monsoon season exceeded the maximum permissible TDS limit (2000 mg/L), total hardness (TH, 600 mg/L), Mg (100 mg/L), and F (1.5 mg/L). Water from these locations may cause gastrointestinal irritation when consumed for drinking. Moreover, 2% of samples exceed the stipulated limit of 400 mg/L for SO_4 and 2% of the samples exceed the permissible limited of TH and F (BIS 2012). The concentrations of SO_4^{2-}, F^-, and TH exceeded the drinking water permissible limit of 200 mg/L, 1.0 mg/L, and 200 mg/L in 8%, 2%, and 2% of the water samples respectively.

Hydrochemical Facies Evaluation

To discern the primary water types, water samples of the two seasons were plotted on the Piper diagram (Piper 1944). Most groundwater and river water samples from both seasons fall in the left quadrant of diamond diagram (Fig. 3a) indicate shallow fresh groundwater ($CaMgHCO_3$) type that is free of contamination, whereas the samples representative of mine water are $CaMgSO_4$ waters. The four post-monsoon

Table 2 Season wise statistical summary of chemical constituents of water samples and compliance in respect of drinking water standards

Chemical Constituent	Pre-monsoon			Post-monsoon			Desirable limit	Permissible limit (PL)	Potential health effect
	Minimum	Maximum	% of the sample above PL	Minimum	Maximum	% of the sample above PL			
pH	3.33	7.87	48.00	3.57	8.06	43.75	6.5–8.5	No relaxation	Taste, corrosion
TDS	41.00	2679.00	4.00	60.40	1015.00	0.00	500	2000	Gastrointestinal Irritation
TH	20.99	1991.70	4.00	21.02	659.65	2.08	200	600	
TA	0.00	200.64	0.00	0.00	112.43	0.00	200	600	
Ca^{2+}	3.87	525.72	4.00	4.26	167.10	0.00	75	200	Scale formation
Mg^{2+}	2.76	165.22	4.00	2.53	68.70	0.00	30	100	–
Na^{+}	1.80	98.10	0.00	3.87	63.75	0.00	–	200[a]	Hypertensive effects
HCO_3^{-}	0.00	250.80		0.00	140.54				
SO_4^{2-}	0.00	2238.40	1.50	0.73	729.04	8.33	200	400	Laxative effect
Cl^{-}	0.90	150.10	0.00	4.00	84.00	0.00	250	1000	Anaesthetic effect, salty taste
NO_3^{-}	0.00	41.58	0.00	0.96	57.87	0.00	45	No relaxation	Methaemoglobinaemia
F^{-}	0.05	2.69	4.00	0.07	1.91	2.08	1	1.5	Skeletal and dental fluorosis

[a]WHO (2011) standards and the rest of the parameters are referred to in BIS 2012. All parameters are in mg/L except pH

groundwater samples tend to fall in the right quadrant (NaCl facies), which are typical of marine and deep ancient ground water. The rest of the samples fall in the top central portion of the diagram, indicating a mixed CaMgCl facies.

Additionally, the samples were plotted on an expanded Durov diagram (Durov 1948) to obtain the processes responsible for the groundwater's chemical evolution. As is evident from Fig. 3b, most of the samples from both seasons fall within field 5, which is due to the mixing of two or more different types of groundwater facies. Similarly, many of the post-monsoon groundwater, river water, and mine water samples and a few pre-monsoon samples fall in field 6, represented by Ca–Mg–HCO_3 type, which is indicative of fresh water and the influence of rock-water interactions in the aquifer. One river water (44) and five mine water (41, 42, 43, 47, 48) samples from both seasons fall in field 2, representative of a Ca-SO_4 facies, and are affected by mine drainage. These sample are acidic in nature with pH < 4 alongside higher TDS values (> 500 mg/L) implies that the mine water is not only influenced by general rock-water interaction mechanism but also affected by AMD. The two post-monsoon GW samples in field 8 represent the rare Na-SO_4 facies and are generally found in an evaporation-dominant environment. The four groundwater samples in field 4 are characterised as Mg–Na–Ca–Cl type and show the possible influence of reverse ion exchange.

Ludwig–Langelier Plot

The Ludwig–Langelier square plot (Langelier and Ludwig 1942) is similar to the projection areas of the Piper and Durov plots. This plot allows one to predict the patterns quickly and correlations between the major cations and anions for multiple samples. Ludwig–Langelier plot of dominant cations and anions ($Ca^{2+} + Mg^{2+}$ vs $HCO_3^{-} + CO_3^{2-}$) at 50% ion balance (cations and anions each 50%) suggests that most of the samples correspond to Ca^{2+}–Mg^{2+}–HCO_3^{-} facies (Fig. 4a) and mixed Ca^{2+}–Mg^{2+}–Cl^{-} facies. It reflects an evolution from the meteoric-derived groundwater (Ca^{2+}–Mg^{2+}–HCO_3^{-}), where the groundwater gets recharged with fresh water without any contamination and then slightly altered to Ca^{2+}–Mg^{2+}–Cl^{-} facies due to reverse ion exchange. However, a Ludwig–Langelier plot (Fig. 4b) of other cations and anions ($Na^{+} + K^{+}$ vs $Cl^{-} + SO_4^{2-}$) shows a slightly increasing trend towards Cl^{-} and SO_4^{2-} with Ca^{2+} and Mg^{2+} dominant cations for mine water and two groundwater and river water samples. This indicates that they originated from other sources, possibly due to the influence of mine drainage water from the dissolution of silicate minerals and small amounts of pyrite in the country rock. Thus, the post-monsoon groundwater samples are enriched with alkalis (Na^{+} and K^{+}) rather than alkaline earth metals (Ca^{2+} and Mg^{2+}) and the reverse is true for pre-monsoon samples. For all of the mine and river water samples, it is evident that the alkaline earth metals (Ca^{2+} and Mg^{2+}) exceed the alkalis

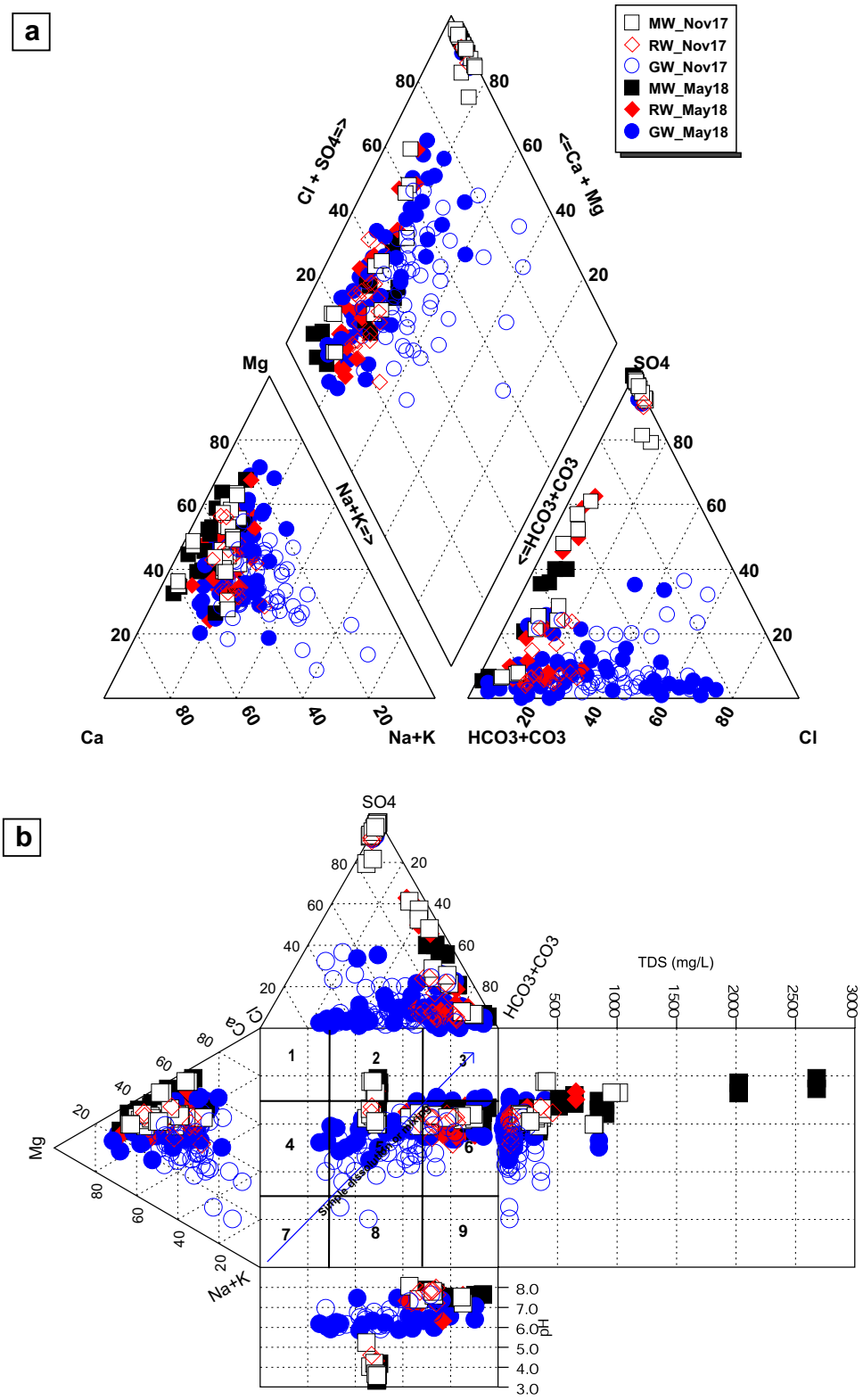

Fig. 3 Evaluation of hydrochemical facies by the **a** Piper trilinear and **b** expanded Durov diagram

(Na^+ and K^+) at all locations for both seasons. However, in the case of anion composition, the mine water samples feature strong acids (Cl^- and SO_4^{2-}) rather than the weak acid (HCO_3^-), while those that tend to fall at the bottom left corner are free from contamination and favour the weak acid (HCO_3^-) rather than Cl^- and SO_4^{2-}. Tthe evolution of surface water is observed to be simple; most of the samples are characterized by one main trend, i.e. less mineralized

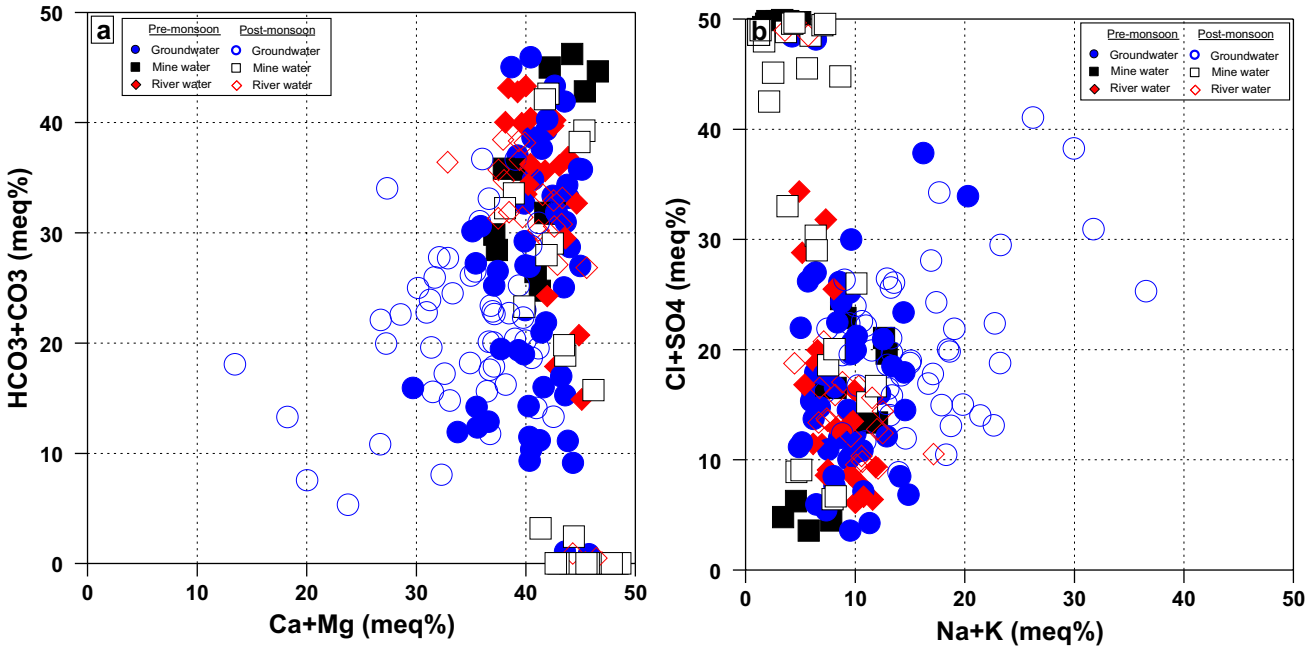

Fig. 4 Ludwig–Langelier plot of **a** dominant cations and anions, and **b** other available cations and anions

Ca^{2+}–Mg^{2+}–HCO_3^- type water with temporary hardness, which indicates recharge from fresh water and less water rock interaction (Handa 1979).

Mine Water Discharge and Dissolved Elemental Fluxes

It is quite common for mining to intercept the water table; as a consequence, groundwater seeps into the mine voids and then the impounded water is discharged to the surface and treated to keep the mine dry and ensure mine safety. At times, the discharge water is used for various purposes such as industrial needs (i.e. the water requirement of the project), domestic and irrigation use of nearby populace. Therefore, it is imperative to check the elemental flux and total solute transfer occurring as a consequence of the annual water discharge from the six mines of the Bishrampur coalfield. Accordingly, the estimated solute loads of 2901 t discharged (Table 3), ranging from 91 t/year (Mahan OC) to 1030 t/year (Bhatgaon UG). Here, the solute delivery rates are interdependent of mine discharge (m^3/year) and elemental fluxes (t/year). The Mahamaya UG mine generates an annual solute load of 984 t despite a meagre mine discharge 1.12×10^6 m^3 and this is attributed to substantial elemental flux or elevated major ion content added to the water by AMD. In terms of season variation, solute loads are mostly from the pre-monsoon (9 t/day) rather than the post-monsoon season (7 t/day), with significant variation in elemental fluxes. The elemental flux data follows the dominance order of $HCO_3^- > SO_4^{2-} > Ca^{2+} > Mg^{2+}$; these four elements together account for 87% and 89% of the total solute fluxes during pre- and post-monsoon seasons, respectively (Table 3). The surplus mine seepage water with solute loads is discharged in natural drains and irrigates the land; this may provide nutrition for the soils, but on the other hand it may affect the growth and yield of crops due to very high sulphate concentrations. However, the conjunctive use of mine discharge water with groundwater and/or surface water will lead to better results.

Acid Mine Drainage (AMD) Role in Solute Acquisition Processes

Based on the major ion chemistry, it seems that some of the mine water samples are influenced by AMD as they have low pH and higher SO_4, EC, and TDS concentrations. Generally, for AMD, coal and associated formations should contain substantial amount of sulfide compounds. However, it is very clear from the geology of the study area that the strata belong to the Lower Gondwana Formations of the Gondwana Super group. The coal from these formations are characterized by high ash, high moisture, and low sulphur content (< 1%) unlike India's tertiary coals (CMPDIL 2014; GSI 1993); thus, the chances for AMD in the area are meagre.

The strong positive correlation of TDS with SO_4^- (Fig. 5a) observed for the three mine water samples, and two river and groundwater samples indicates the influence of AMD. Likewise, the scatter plot of SO_4^- vs Ca^{2+}/SO_4^- (molar ratios) (Fig. 5b) exemplifies that the AMD-contaminated water tends to fall parallel to the X-axis

Table 3 Annual mine water discharge and elemental flux estimated for the six mines of the Bishrampur Coalfield, central India, before (pre-) and after (post-) the monsoon

Mine name	Average mine discharge (m^3/day)	Season	Dissolved elemental flux discharge (t/day)										Total solute flux (t/day)	Average annual solute flux (t/year)
			Ca^{2+}	Mg^{2+}	Na^{+}	K^{+}	HCO_3^{-}	SO_4^{2-}	Cl^{-}	NO_3^{-}	F^{-}	TZ^{+}	TZ^{-}		
Mahan II OC	1973	Pre-	0.073	0.040	0.046	0.014	0.315	0.155	0.021	0.005	0.000	0.173	0.496	0.669	244.19
		Post-	0.070	0.046	0.032	0.017	0.269	0.214	0.016	0.005	0.001	0.164	0.505	0.669	
Nawapara UG	6133	Pre-	0.103	0.110	0.044	0.028	0.897	0.040	0.023	0.006	0.002	0.286	0.967	1.253	404.05
		Post-	0.094	0.062	0.025	0.030	0.670	0.039	0.031	0.008	0.002	0.211	0.751	0.961	
Shivani UG	1916	Pre-	0.048	0.021	0.023	0.012	0.254	0.057	0.013	0.002	0.001	0.104	0.328	0.432	148.18
		Post-	0.046	0.016	0.018	0.012	0.206	0.062	0.015	0.003	0.001	0.092	0.288	0.380	
Bhatgaon UG	6778	Pre-	0.547	0.261	0.096	0.049	0.000	2.471	0.025	0.012	0.003	0.953	2.511	3.465	1029.90
		Post-	0.288	0.157	0.101	0.049	0.128	1.243	0.136	0.073	0.004	0.595	1.583	2.179	
Mahan OC	133	Pre-	0.061	0.021	0.005	0.002	0.000	0.280	0.000	0.000	0.000	0.090	0.281	0.371	90.80
		Post-	0.018	0.007	0.001	0.001	0.000	0.097	0.002	0.001	0.000	0.027	0.100	0.127	
Mahamaya UG	3262	Pre-	0.357	0.212	0.053	0.026	0.000	2.095	0.020	0.002	0.003	0.647	2.119	2.766	984.23
		Post-	0.261	0.213	0.095	0.040	0.000	1.994	0.020	0.003	0.002	0.608	2.019	2.627	

(ordinance) and non-contaminated water samples, mostly GW, RW, and a few MW, fall parallel to the Y-axis with low SO_4^{-} content. The plot of pH vs Ca^{2+}/SO_4^{-} (molar ratios) was made to check the presence of AMD followed by carbonate neutralisation (Fig. 5c), in which samples fall in the field near the Ca^{2+}/SO_4^{-} molar ratio of 2 (Wu et al. 2009). The plot reveals that no significant carbonate buffering occurred, and AMD was noticed for most of the groundwater, river water, and a few mine-water samples with a Ca^{2+}/SO_4^{-} molar ratio more than 3 and pH > 6.5. However, the mine water from the Bhatgaon UG, Mahan OC, and Mahanaya UG mines and surrounding groundwater and river water samples are strongly influenced by AMD. There is also a clear indication of carbonate buffering of these AMD-influenced samples, probably by dolomite and calcite dissolution (Eq. 2). Dissolution of aluminosilicates (Arkosic sandstone), which are predominant in the area, also played a major role in the dominance of Ca and other constituents.

$$FeS_2 + 3.75O_2 + 3.5H_2O + 4CaCO_3 \rightarrow Fe(OH)_3 + 4HCO_3^{-} + 2SO_4^{2-} + 4Ca^{2+} \quad (2)$$

It is pertinent to mention here that the AMD in the mine water samples and adjacent groundwater samples are closely related to the geology. Here, AMD was only dominant in three mines namely Bhatgaon UG, Mahan OC, and Mahamaya UG mines out of six operational mines and incidentally, these three mines are on the verge of the basin boundary (Fig. 1): i.e. mines affected by AMD are in the transition zone of Barakar and Talchir Formation and/or metamorphic rock units. It can therefore be concluded that AMD is a dominant process in these mines, along with carbonate dissolution, whereas dissolution of aluminosilicates is the key process that controls the water chemistry of the rest of the area in addition to elevated CO_2 in the soil zone of the weathered-mantle (WM).

To trace the probable processes responsible for the variations in the area's water chemistry, the plots of Na-normalized Ca^{2+} vs Mg^{2+} (Fig. 6a) and Na-normalized Ca^{2+} vs HCO_3 (Fig. 6b) molar ratios on log–log scale bivariate plot exhibits that most groundwater samples fall near the field of silicate weathering due to lower Mg^{2+}/Na^{+} and Ca^{2+}/Na^{+} ratios. On the other hand, river water appears in the transition between silicate weathering and carbonate dissolution while the mine water samples also have an analogous pattern, but slightly offset towards carbonate dissolution. The elevated Mg^{2+}/Na^{+}, Ca^{2+}/Na^{+}, and HCO_3^{-}/Na^{+} ratios in these samples are ascribed to mixing and carbonate dissolution coupled with trivial silicate weathering.

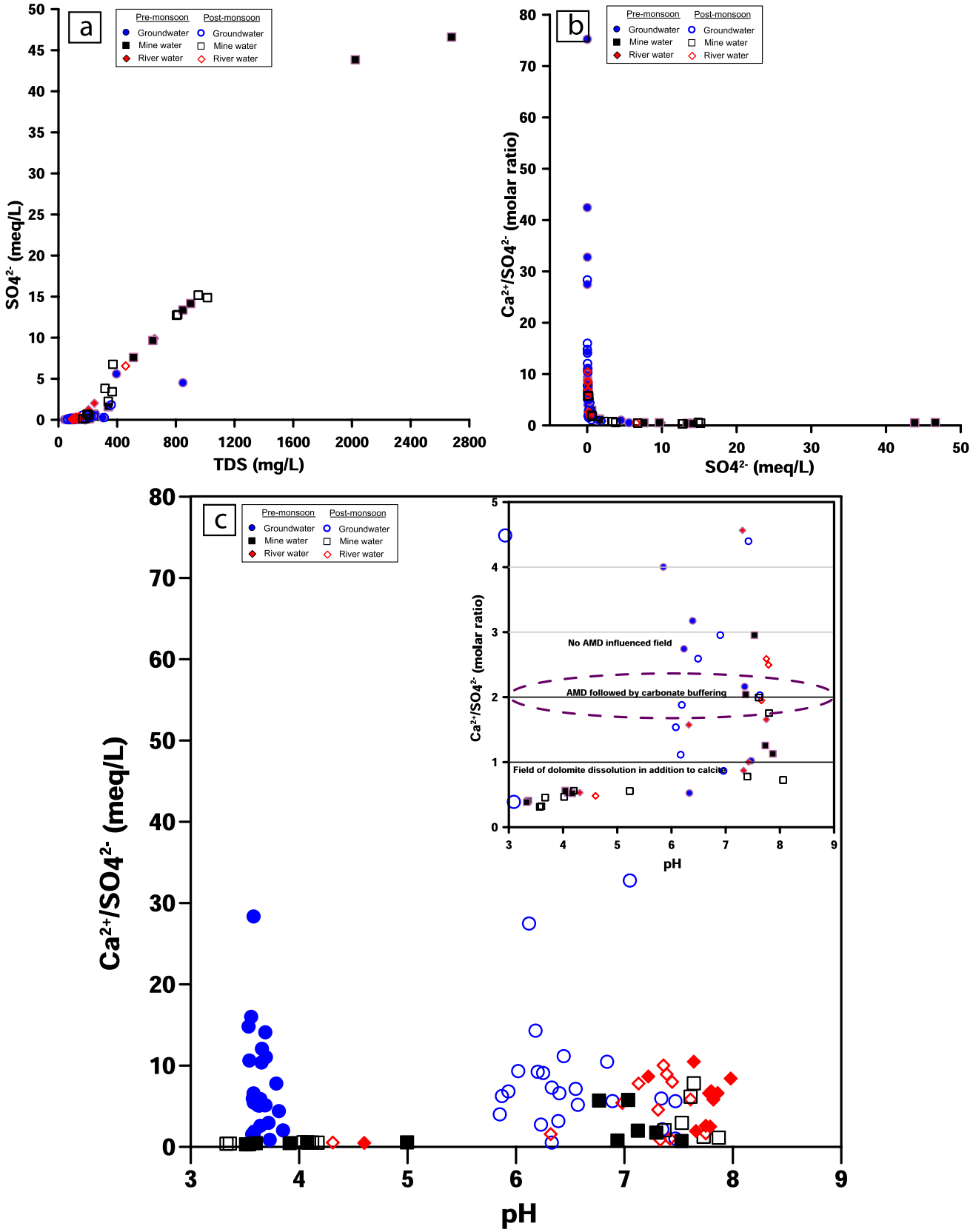

Fig. 5 The scatter plot of **a** TDS with SO_4, **b** SO_4 vs Ca/SO_4 (molar ratios) and **c** pH vs Ca/SO_4 exemplifies the AMD influence in the area

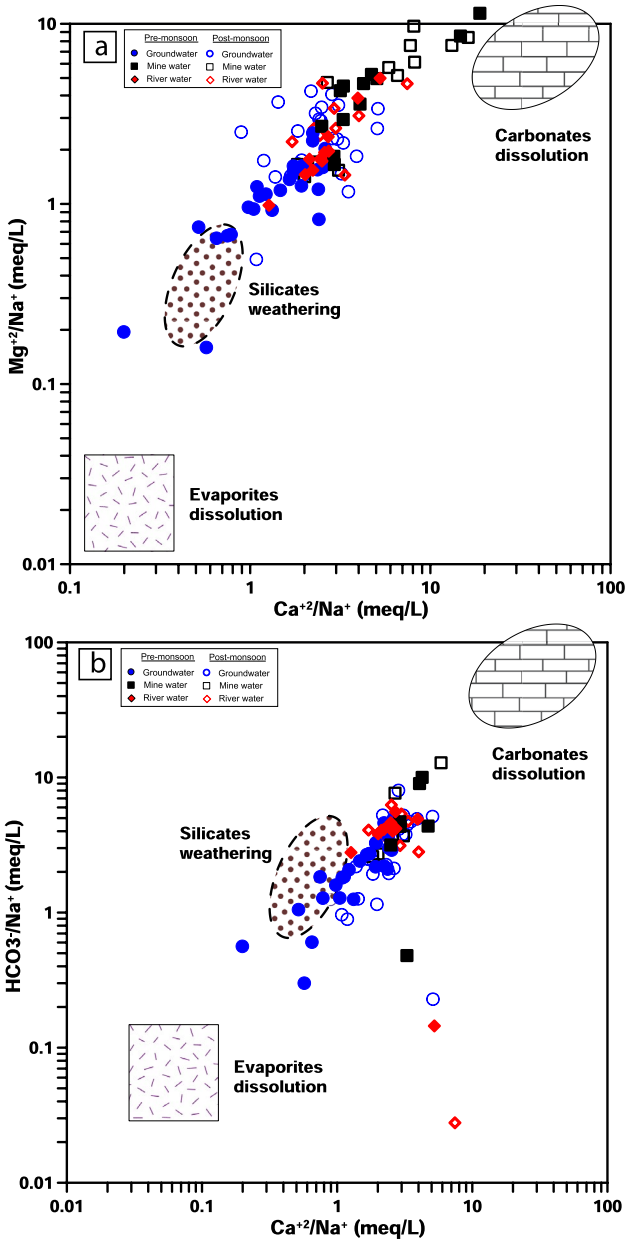

Fig. 6 Bivariate Na-normalized molar ratios mixing diagram **a** Ca vs Mg, **b** Ca vs HCO_3, illustrating the three end-members (carbonates, silicates, and evaporites)

Solute Source Identification

The potential source of pollutants and their distribution in the multidimensional space and time was appraised using chemometric methods such as principal component analysis (PCA) and both R and Q-mode hierarchical cluster analysis (HCA).

Principal Component Analysis (PCA)

PCA is an effective data reduction tool performed to determine the key factors contributing to potential sources of variation in the hydrochemistry of water resource of the study area. Based on the criteria addressed in the methodology section, 14 parameters (pH, EC, TDS, F^-, Cl^-, HCO_3^-, SO_4^{2-}, NO_3^-, Ca^{2+}, Mg^{2+}, Na^+, K^+, TH, and TA) were chosen for multivariate statistical processing (PCA) and eventually three factors with eigenvalues > 1 are extracted sequentially through the varimax rotation and that accounts for 92.17% and 85.43% of the total variation for the pre- and post- monsoon seasons, respectively (Table 4). For the better visual summary of these components loadings, they are shown in Fig. 7.

The first component (PC1) is strongly correlated (> 0.5) with variables EC, TDS, F^-, SO_4^{2-}, Ca^{2+}, Mg^{2+}, Na^+, K^+, and TH, which explain about 56.5% of the variance for the pre-monsoon and 46.6% for the post-monsoon season. This component is related to dissolution of carbonates and silicate weathering along its flow path, as indicated by the higher loadings of Ca^{2+}, Mg^{2+}, Na^+, K^+ ions, and TH. However, the togetherness of EC, TDS, and SO_4^{2-} in PC1 is ascribed to possible AMD in the mine water samples in addition to carbonate buffering and silicate dissolution. Hence, the PC1 is regarded as a geogenic source governing the water chemistry of these variables and the significant loading of F^- (0.82) for pre-monsoon supports this statement since the occurrence of fluoride in groundwater mostly has a geogenic origin (Kumar et al. 2019). Moreover, comparatively lower loading exhibited by most of the parameters during post-monsoon is portraying the dilution effect due to ample rain fall in the study area.

The PC2 shows strong positive correlation with pH but a strong negative correlation with HCO_3^- and TA with 23.39% and 21.12% of the variance in the hydrochemistry for pre- and post-monsoon seasons, respectively. The significant negative correlation observed between pH and HCO_3^- is attributed to CO_2 dissolving to form carbonic acid, which is a weak, unstable acid and soon gets converted into HCO_3^-, decreasing the pH (Drever 1997). Finally, the elevated bicarbonate and TA reported in PC2 are representative of meteoric origin alongside host rock and weathered mantle dissolution.

The final component (PC3) has a prominent loading for Cl^-, NO_3^-, and Na^+ and represents the least variance of 12.27% and 17.73% respectively, for pre- and post-monsoon seasons. It represents the influence of local anthropogenic inputs such as discrete discharge of fertilizers used in the agricultural fields for cultivation purpose, the wastewater from the septic tanks and animal wastes (Devic et al. 2014; Kumar et al. 2018). This effect is prominent during post-monsoon in comparison to that of pre-monsoon and which

Table 4 Results of PCA for pre and pot-monsoon seasons indicating three clusters

Parameters	Pre-monsoon			Post-monsoon		
	PC1	PC2	PC3	PC1	PC2	PC3
pH	0.07	**0.97**	0.09	0.19	**0.88**	0.34
EC	**0.97**	0.21	0.08	**0.93**	0.31	0.10
TDS	**0.98**	0.18	0.02	**0.96**	0.24	0.04
F^-	**0.82**	0.12	−0.29	0.41	0.18	−0.48
Cl^-	0.24	−0.23	**0.86**	0.15	−0.07	**0.91**
HCO_3^-	−0.32	**−0.94**	0.03	−0.38	**−0.91**	0.10
SO_4^{2-}	**0.89**	0.30	−0.16	**0.92**	0.26	−0.07
NO_3^-	−0.19	0.31	**0.85**	−0.13	0.20	**0.87**
Ca^{2+}	**0.96**	0.19	−0.04	**0.95**	0.21	−0.05
Mg^{2+}	**0.92**	0.31	0.00	**0.90**	0.32	−0.08
Na^+	**0.92**	−0.13	0.28	**0.62**	0.06	**0.58**
K^+	**0.85**	0.10	0.21	**0.62**	0.13	0.41
TH	**0.96**	0.25	−0.02	**0.94**	0.26	−0.06
TA	−0.30	**−0.95**	0.03	−0.37	**−0.91**	0.10
% of Variance	56.51	23.39	12.27	46.57	21.12	17.73
Cumulative %	56.51	79.90	92.17	46.57	67.69	85.43
KMO and Bartlett's test						
Sampling adequacy	0.80			0.74		
Approx. Chi-square	1733.57			1503.48		
df	91.00			91.00		
Sig.	0.00			0.00		

The bold values indicate higher loadings

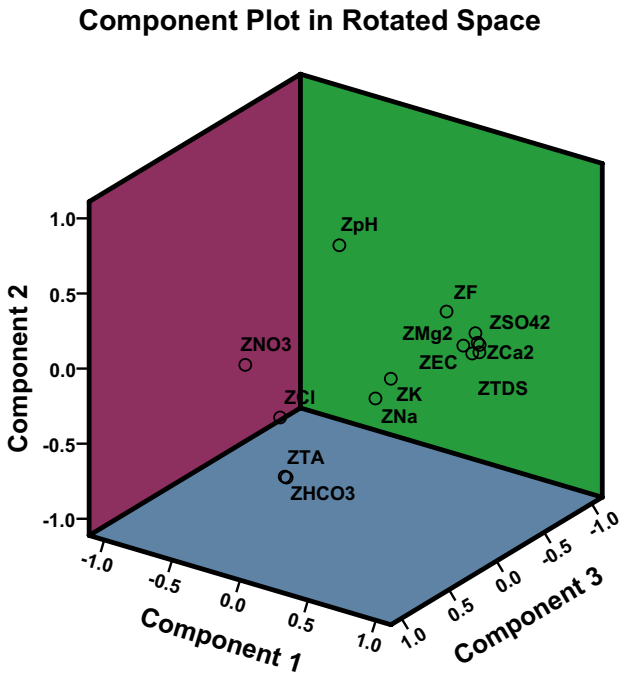

Fig. 7 Principal component analysis plot of physicochemical parameters

has been witnessed by significant loading of Na^+ (0.58) in association with Cl^- (0.91), and NO_3^- (0.87). Overall, there was not much seasonal variation noted from the PCA in terms of geochemical processes, but it indicates that anthropogenic aspects control the geochemistry of the water resources.

Hierarchical Cluster Analysis (HCA)

Initially, the R-mode HCA was run separately for both pre- and post-monsoon seasons using the same 14 parameters as above. The results of R-mode HCA are illustrated as a dendrogram plot (Fig. 8a) that reveals that the physicochemical components are seasonally grouped into three main water groups.

The first cluster constructed with HCO_3^- and TA is related to the infiltrating precipitation interacting with the weathered mantle. The second cluster shows the association of Cl^-, NO_3^-, Na^+, K^+, and pH, which are probably due to anthropogenic activities. The final cluster, with EC, TDS, F^-, SO_4^{2-}, Ca^{2+}, Mg^{2+}, and TH, represent the process of dissolution of carbonates and silicates in addition to sulphide mineral weathering. The results of the R-mode HCA concur with the PCA and aforementioned hydrochemical processes. Likewise, the dendrogram for the Q-mode HCA reveals three hydrochemical spatial relationships based on similarities of water quality characteristics (Fig. 8b).

Cluster 1 is comprised of mine water samples from the Nawapara UG, Shivani UG, and Mahan-II OC mines as well

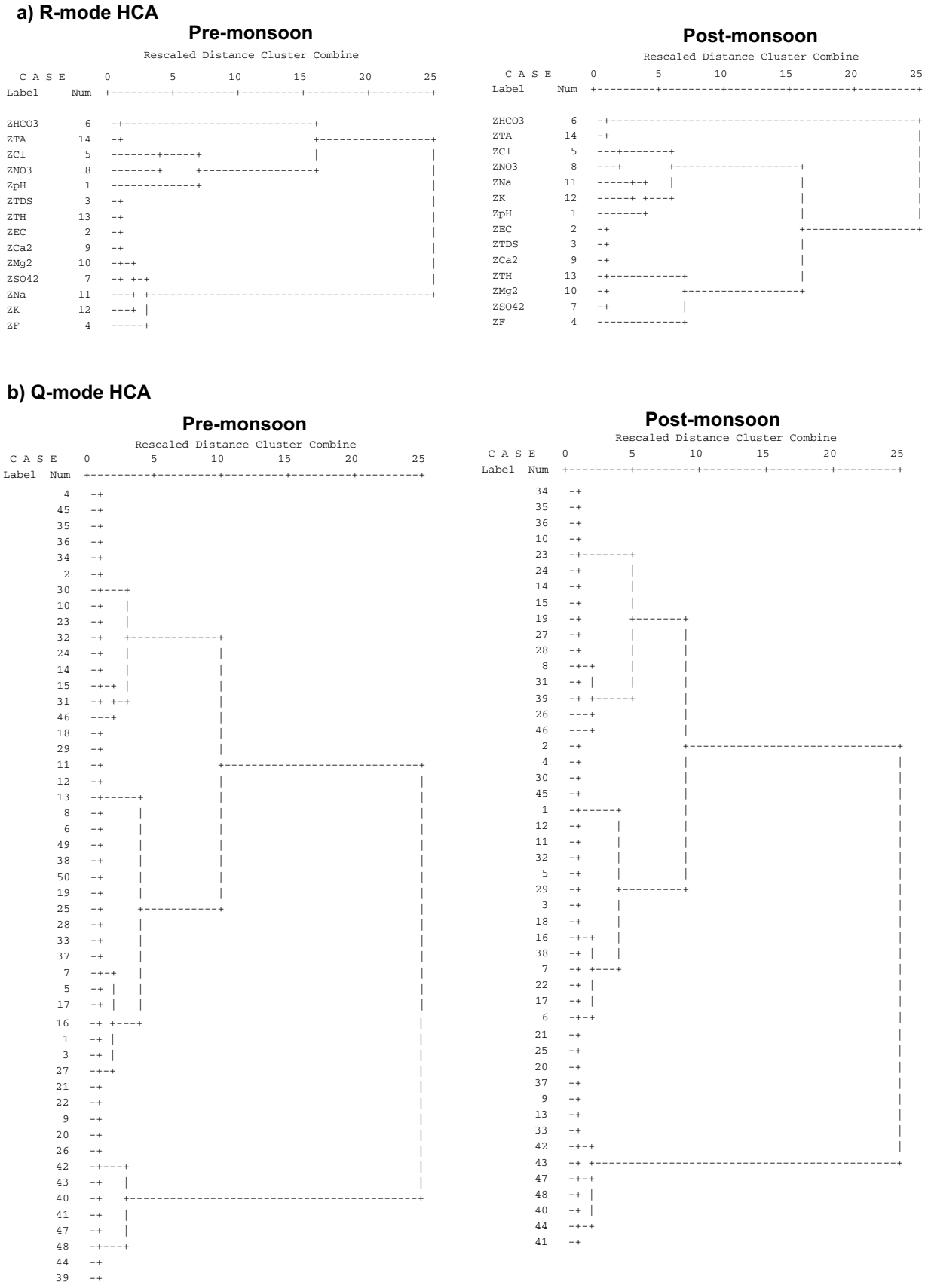

Fig. 8 Dendrogram generated from HCA of water chemistry with respect to measured physicochemical parameters (R-mode) data and the sampling sites (Q-mode)

as nearby groundwater sampling sites; most of these stations show low concentrations of all the ions, including TDS. The mine water samples from this cluster are indicative of no AMD contamination. Cluster 2 consists of river water and its proximate groundwater samples and this might be considered an unpolluted zone. Particularly, two stations situated at higher elevation collected during the pre-monsoon season shows low elemental ratios with TDS < 100, representing fresh water free from contamination (Freeze and Cherry 1979; Shen et al. 1993). Finally, cluster 3 can be regarded as the most polluted zone due to AMD in the mine water samples of the Bhatgaon UG, Mahamaya UG, and Mahan OC mines along with a few groundwater samples located near these mines and river water samples. All these stations exhibit higher concentrations of TDS and major ion constituents than the other two clusters, indicating that the mine water samples of cluster 3 are affected by AMD in addition to mineral dissolution.

Conclusion

In the present study, the geochemical evolution of groundwater and the impacts of anthropogenic changes and mine water, river water, and groundwater interactions were studied based on different hydrochemical models and ion ratios. Overall, there exists a seasonal variation in groundwater and river water chemistry in the area but can be regarded as relatively fresh with characteristic of Ca-Mg-HCO_3 facies. However, the mine water samples (R43, 42) from both the seasons are representative of Ca-Mg-SO_4 facies and which are acidic in nature with pH < 4 along with high concentration of SO_4 and TDS values (> 500 mg/L) suggests that they are influenced by AMD alongside general rock-water interaction mechanism. The bivariate plots made based on molar ratios SO_4 vs Ca/SO_4, pH vs Ca/SO_4 and TDS, with SO_4 indicate that oxidation of sulfide compounds in the coal and coal measure rocks is the governing process controlling AMD generation (Bhatgaon UG, Mahamaya UG, and Mahan OC mines) and groundwater and river water close to these collieries. In contrast, water samples from major rivers and groundwater from the study area are not much influenced by AMD. The PCA and HCA results substantiate the solute acquisition interpretations and confirm that the geogenic processes in general control the water chemistry of the area. This, in turn, could be the plausible reason, alongside the effectiveness of the measures implemented by the project authority, for the overall good quality of the water resources in the study area despite mining activity. However, a few mine water and adjacent groundwater and river water samples are mildly affected by anthropogenic inputs (i.e. coal mining).

Acknowledgements The authors are very grateful to the management of CMPDIL, Ranchi, SECL, Bilaspur and AKS University, Satna for the facilities extended towards the publication of this paper. We also thank the CSIR-Central Institute of Mining and Fuel Research, Dhanbad, for some of the analytical support. The views expressed in this paper are of the authors only and not necessarily of the organizations to which they belong.

References

Acharya BS, Kharel G (2020) Acid mine drainage from coal mining in the United States—an overview. J Hydrol. https://doi.org/10.1016/j.jhydrol.2020.125061

Agarwal RP, Dotiwala SF, Bhoj R (1993) Structural framework of Son-Mahanadi Gondwana basin based on the study of remote sensing data. Gondwana Geol Mag, Special Vol., National Symp Gondwana, pp 207–217

APHA (American Public Health Association) (2012) Standard methods for the examination of water and waste water. APHA, Washington, DC

BIS (Bureau of Indian Standards) (2012) IS: 10500, Indian Standard for Drinking Water Specification. 2nd Revision, New Delhi

CMPDIL (Central Mine Planning and Design Institute Ltd.) (2014) Geological Report on Coal Exploration Gevra, Dipka, Hardi, Ponri, Naraibodh- I & Naraibodh-II combined block, Korba coalfield, Korba (C.G.), India. CMPDIL, Coal India Ltd., India

Devic G, Djordjevic D, Sakan S (2014) Natural and anthropogenic factors affecting the groundwater quality in Serbia. Sci Total Environ 468(469):933–942

Drever JI (1997) The geochemistry of natural waters: surface and groundwater environments. Prentice Hall, New Jersey

Durov SA (1948) Classification of natural waters and graphic representation of their composition. Doklady Akad Nauk USSR 59:87–90

Freeze JA, Cherry RA (1979) Groundwater, 1st edn. Prentice Hall, New Jersey

GSI (Geological Survey of India) (1993) Final Report on Regional Exploration for Coal in the Bhelai East Area, South Central Part of Korba Coalfield, Bilaspur District, M.P., India

Handa BK (1979) Groundwater pollution in India. In: Proc National Symp on Hydrology, IAHS, Univ of Roorkee, India, pp 34–49

Kumar S, Venkatesh AS, Singh R, Udaybhanu G, Saha D (2018) Geochemical signatures and isotopic systematics constraining dynamics of fluoride contamination in groundwater across Jamui District, Indo-Gangetic alluvial plains, India. Chemosphere. https://doi.org/10.1016/j.chemosphere.2018.04.116

Kumar S, Singh R, Venkatesh AS, Udayabhanu G, Sahoo PR (2019) Medical geological assessment of fluoride contaminated groundwater in parts of Indo-Gangetic Alluvial plains. Sci Rep 9:16243. https://doi.org/10.1038/s41598-019-52812-3

Langelier W, Ludwig H (1942) Graphical methods for indicating the mineral character of natural waters. J Am Water Assoc 34:335–352

Mahato MK, Singh G, Singh PK, Singh AK, Tiwari AK (2017) Assessment of mine water quality using heavy metal pollution index in a coal mining area of Damodar River Basin, India. Bull Environ Contam Toxicol 99:54–61. https://doi.org/10.1007/s00128-017-2097-3

Piper AM (1944) A graphic procedure in geochemical interpretation of water analysis. Trans Am Geophys Union 25:914–923

Ray S, Dey K (2020) Coal mine water drainage: the current status and challenges. J Inst Eng India Ser D 101:165–172. https://doi.org/10.1007/s40033-020-00222-5

Shen ZL, Zhu WH, Zhong Z (1993) Basics of Hydrogeochemistry. Geol Press, Beijing **(in Chinese)**

Singh R, Syed TH, Kumar S, Kumar M, Venkatesh AS (2017a) Hydrogeochemical assessment of surface and groundwater resources of Korba coalfield, Central India: environmental implications. Arab J Geosci 10:318. https://doi.org/10.1007/s12517-017-3098-6

Singh R, Venkatesh AS, Syed TH, Reddy AGS, Kumar M, Kurakalva RM (2017b) Assessment of potentially toxic trace elements contamination in groundwater resources of the coal mining area of the Korba Coalfield, Central India. Environ Earth Sci https://doi.org/10.1007/s12665-017-6899-8

Singh R, Venkatesh AS, Syed TH, Surinaidu L, Pasupuleti S, Rai SP, Kumar M (2018) Stable isotope systematic and geochemical signatures constraining groundwater hydraulics in the mining environment of the Korba Coalfield, Central India. Environ Earth Sci 77:548. https://doi.org/10.1007/s12665-018-7725-7

Singh R, Gayen A, Kumar S, Dewangan R (2021a) Geospatial distribution of arsenic contamination of groundwater resources in intricate crystalline aquifer system of Central India: arsenic toxicity manifestation and health risk assessment. Hum Ecol Risk Assess. https://doi.org/10.1080/10807039.2020.1865787

Singh R, Narayan ID, Doley T, Kumar N, Bandyopadhyay D, Kisku DK (2021b) Climate-resilient groundwater rationing in the mining environment: an operational framework from India. Environ Earth Sci. https://doi.org/10.1007/s12665-021-09732-1

Suhag R (2016) Overview of Ground Water in India. PRS Legislative Research. https://prsindia.org/files/policy/policy_analytical_reports/1455682937-Overview%20of%20Ground%20Water%20in%20India_0.pdf

Tziritis E, Skordas K, Kelepertsis A (2016) The use of hydrogeochemical analyses and multivariate statistics for the characterization of groundwater resources in a complex aquifer system. A case study in Amyros River basin, Thessaly, central Greece. Environ Earth Sci 75:339. https://doi.org/10.1007/s12665-015-5204-y

Wagh VM, Panaskar DB, Jacobs JA, Mukate SV, Muley AA, Kadam AK (2019) Influence of hydro-geochemical processes on groundwater quality through geostatistical techniques in Kadava River basin, western India. Arab J Geosci 12:7. https://doi.org/10.1007/s12517-018-4136-8

WHO (2011) Guidelines for, drinking-water quality, 4th edn. World Health Organization, Geneva

Wu P, Tang C, Liu C, Zhu L, Pei T, Feng L (2009) Geochemical distribution and removal of As, Fe, Mn and Al in a surface water system affected by acid mine drainage at a coalfield in southwestern China. Environ Geol 57:1457–1467. https://doi.org/10.1007/s00254-008-1423-9